Inorganic Chemistry

Article

pubs.acs.org/IC

Quaternary Arsenides $AM_{1.5}Tt_{0.5}As_2$ (A = Na, K, Rb; M = Zn, Cd; Tt = Si, Ge, Sn): Size Effects in $CaAl_2Si_2$- and $ThCr_2Si_2$-Type Structures

Mansura Khatun, Stanislav S. Stoyko, and Arthur Mar*

Department of Chemistry, University of Alberta, Edmonton, Alberta, Canada T6G 2G2

Supporting Information

ABSTRACT: Ten quaternary arsenides $AM_{1.5}Tt_{0.5}As_2$ (A = Na, K, Rb; M = Zn, Cd; Tt = Si, Ge, Sn) have been prepared by stoichiometric reactions of the elements at 600−650 °C. Seven of them ($NaZn_{1.5}Si_{0.5}As_2$, $NaZn_{1.5}Ge_{0.5}As_2$, $NaZn_{1.5}Sn_{0.5}As_2$, $NaCd_{1.5}Sn_{0.5}As_2$, $KZn_{1.5}Sn_{0.5}As_2$, $KCd_{1.5}Sn_{0.5}As_2$, $RbCd_{1.5}Sn_{0.5}As_2$) adopt the trigonal $CaAl_2Si_2$-type structure (Pearson symbol $hP5$, space group $P\bar{3}m1$, Z = 1, a = 4.0662(3)−4.4263(7) Å, c = 7.4120(5)−8.4586(14) Å), whereas the remaining three ($KZn_{1.5}Si_{0.5}As_2$, $KZn_{1.5}Ge_{0.5}As_2$, $RbZn_{1.5}Ge_{0.5}As_2$) adopt the tetragonal $ThCr_2Si_2$-type structure (Pearson symbol $tI10$, space group $I4/mmm$, Z = 2, a = 4.0613(10)−4.1157(5) Å, c = 14.258(3)−14.662(2) Å). Both structure types contain anionic $[M_{1.5}Tt_{0.5}As_2]$ slabs that are built from edge-sharing tetrahedra and that stack alternately with nets of A cations. A structure map delineates the formation of these structure types for $AM_{1.5}Tt_{0.5}As_2$ as a function of simple radius ratios. Although these arsenides have charge-balanced formulations, band structure calculations on $NaZn_{1.5}Tt_{0.5}As_2$ (Tt = Si, Ge, Sn) indicate that semimetallic behavior is predicted as a result of overlap of the valence and conduction bands.

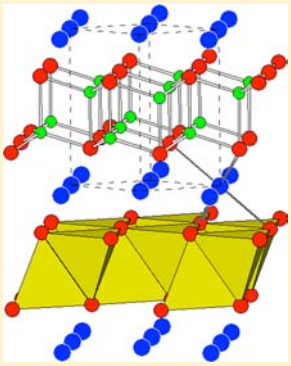

INTRODUCTION

Ternary phases AB_2X_2 are formed for many combinations of components A (alkali, alkaline-earth, or rare-earth metal), B (transition metal or main-group metalloid), and X (element from groups 13−16).[1] Most adopt the tetragonal $ThCr_2Si_2$-type structure, which serves as the prototype for many materials with interesting physical properties such as superconductivity (e.g., doped $BaFe_2As_2$).[2] However, many also adopt the trigonal $CaAl_2Si_2$-type structure, which appears to be more limited because of stricter electronic requirements. With few exceptions, the valence electron count must satisfy 16 e^-/f.u. and the B component should have filled or half-filled d-electron configurations (d^0, d^5, or d^{10}).[3−10] Because these conditions typically lead to small band gap semiconducting behavior, these compounds have been identified as promising candidates for thermoelectric materials (e.g., doped $YbZn_2Sb_2$ and $YbCd_2Sb_2$).[11−15] Notwithstanding these restrictions, there is still a wide variety of A, B, and X components that can be chosen while maintaining charge balance. In fact, quaternary representatives of the $CaAl_2Si_2$-type structure can be prepared through appropriate aliovalent substitution, as exemplified by our recent investigation of the quaternary rare-earth phosphides $RECuZnP_2$ in which Cu and Zn atoms are disordered over the single B site.[16] In hopes of expanding the versatility of the $CaAl_2Si_2$-type structure, we are interested in exploring what other combinations of metal components A and B could be successful in affording further quaternary representatives.

We report here the synthesis of new quaternary arsenides $AM_{1.5}Tt_{0.5}As_2$ derived from combinations of an alkali metal (A = Na, K, Rb), a group-12 metal (M = Zn, Cd), and a tetrel (Tt = Si, Ge, Sn). They segregate into two groups, adopting either $CaAl_2Si_2$- or $ThCr_2Si_2$-type structures. Because the valence electron count is constant (16 e^-/f.u.), an attractive opportunity is available to examine the size effects that influence the formation of the $CaAl_2Si_2$- vs $ThCr_2Si_2$-type structures in this series of compounds. Their bonding and electronic structures are further analyzed through band structure calculations.

EXPERIMENTAL SECTION

Synthesis. Starting materials were Na, K, and Rb pieces; Zn and Cd shot; Si, Ge, and Sn ingots or granules; and As lumps; all with purities greater than 99.9% and obtained from Alfa-Aesar, Aldrich, or other local sources. All reagents and products were handled within an argon-filled glovebox. Stoichiometric mixtures of the elements were loaded into alumina crucibles placed within fused-silica tubes, which were evacuated and sealed. The tubes were heated to 650 °C (for Na and K samples) or 600 °C (for Rb samples) over 2 d, held at that temperature for 10 d, and cooled to room temperature over 2 d. A different annealing temperature was used for the Rb samples because of the low boiling point for Rb metal (688 °C). The products were moderately air-sensitive, with the surfaces of crystals becoming visibly tarnished within minutes, and were thus handled under paraffin oil. Powder X-ray diffraction (XRD) patterns were collected on an Inel diffractometer equipped with a curved position-sensitive detector (CPS 120) and a Cu $K\alpha_1$ radiation source operated at 40 kV and 20 mA. They confirmed that the quaternary arsenides $AM_{1.5}Tt_{0.5}As_2$ were generally formed as the major phase in each reaction, with ternary arsenides AM_4As_3 and $A_2M_5As_4$ found as the most common secondary phases.[17,18] Representative powder XRD patterns are provided in Figure S1 in Supporting Information. Quantitative yields were difficult to achieve because many of the elemental components (particularly the alkali metals, Zn, Cd, Sn, and As) as well as possible intermediate

Received: November 30, 2012
Published: March 4, 2013

   dx.doi.org/10.1021/ic302627n | Inorg. Chem. 2013, 52, 3148−3158

binary phases (e.g., Zn_3As_2, Cd_3As_2, $ZnAs_2$, $CdAs_2$) are highly volatile, which posed problems in maintaining the correct overall composition of the melt. To account for mass balance, Si- or Ge-containing phases may be present in amorphous form, but these would be masked under the large background (subtracted from the patterns) resulting from the paraffin oil. Single crystals of the title compounds were selected under paraffin oil and their chemical compositions were determined by energy-dispersive X-ray (EDX) analysis on a JEOL JSM-6010LA scanning electron microscope. Representative SEM images of these crystals are shown in Figure S2 in Supporting Information. The EDX results, averaged over multiple spectra for several crystals of each compound, are summarized in Table S1 in Supporting Information. In those cases where peaks belonging to different elements overlap in the EDX spectra, the combined atomic percentages were calculated. In general, the experimental compositions for $AM_{1.5}Tt_{0.5}As_2$ were within 1−2 at. % of the expected values (20% *A*, 30% *M*, 10% *Tt*, 40% As). The observation of precise compositions for these crystals, which were selected from products containing mixtures of phases, implies that the quaternary arsenides $AM_{1.5}Tt_{0.5}As_2$ do not exhibit homogeneity ranges.

Structure Determination. Single crystals were selected under paraffin oil, mounted on glass fibers, and placed under a cold nitrogen gas stream on a Bruker PLATFORM diffractometer equipped with a SMART APEX II CCD detector and a Mo Kα radiation source. Full spheres of intensity data were collected at −100 °C using ω scans with a scan width of 0.3° and an exposure time of 12−15 s per frame in 5−7 batches. Face-indexed numerical absorption corrections were applied. Structure solution and refinement were carried out with use of the *SHELXTL* (version 6.12) program package.[19]

For seven of the quaternary arsenides $AM_{1.5}Tt_{0.5}As_2$, the trigonal space group $P\bar{3}m1$ was chosen and the initial atomic positions found by direct methods were consistent with the $CaAl_2Si_2$-type structure.[20] In this structure type normally adopted by ternary phases AB_2X_2, there are three sites available to accommodate the *A*, *B*, and *X* components. We assumed that the group-12 transition metal (*M* = Zn, Cd) and tetrel (*Tt* = Si, Ge, Sn) atoms were disordered within the single available *B* site (at Wyckoff position 2*d*: 1/3, 2/3, ∼0.6). However, the appropriate treatment of disorder depended on the particular combination of *M* and *Tt* atoms, which we detail separately on a case-by-case basis below. Each case is instructive for the crystallographic problems posed. Crystal data and further experimental details are given in Table 1.

For $NaZn_{1.5}Ge_{0.5}As_2$, $KCd_{1.5}Sn_{0.5}As_2$, and $RbCd_{1.5}Sn_{0.5}As_2$, the *M* and *Tt* components differ by only two in atomic number and their X-ray scattering factors are too similar to permit discrimination. If the occupancies of *M* and *Tt* atoms within the *B* site were allowed to vary freely, with the constraint that they sum to unity but with no consideration placed on overall charge balance in the formula, the refinements were generally unstable. In some cases, carefully introducing damping in the refinements eventually led to convergence, but the uncertainties in the occupancies were either large or the resulting formula deviated significantly from expectations (e.g., "$KCd_{1.67(2)}Sn_{0.33(2)}As_2$"), in contradiction to the EDX results. Thus, the occupancies were fixed to be exactly 0.75 *M* and 0.25 *Tt* within this *B* site in the final refinements of these structures.

For $NaZn_{1.5}Si_{0.5}As_2$ and $KZn_{1.5}Sn_{0.5}As_2$, the *M* and *Tt* components should be easily distinguishable by their X-ray scattering factors. When their occupancies within the *B* site were freed, they converged to 0.736(5) Zn/0.264(5) Si and 0.816(15) Zn/0.184(15) Sn, resulting in the formulas $NaZn_{1.47(1)}Si_{0.53(1)}As_2$ and $KZn_{1.63(3)}Sn_{0.37(3)}As_2$, respectively. The former is reasonable, whereas the latter deviates a bit far from expectations. Subsequently, an analysis of the crystallographic data (including structure factors) through checkCIF alerted us to the possibility of merohedral twinning (related by reflection normal to the *c*-axis). This twin component was minor (BASF of 0.03) but its inclusion dramatically cleaned up the difference electron density map and led to occupancies within the *B* site of 0.769(6) Zn/0.232(6) Sn, corresponding to a formula, $KZn_{1.54(1)}Sn_{0.46(1)}As_2$, that is closer to expectations.

For $NaZn_{1.5}Sn_{0.5}As_2$ and $NaCd_{1.5}Sn_{0.5}As_2$, a further complication emerged in which a residual peak (6.0−8.0 $e^-/Å^3$) in the difference electron density map is found close to the *B* site. This site was thus split into two closely separated ones, now labeled *B*1 (the original site at 1/3, 2/3, ∼0.6 with tetrahedral coordination) and *B*2 (a minor site at 1/3, 2/3, ∼0.7 with trigonal planar coordination). Taking into account reasonable bond lengths, we proposed a structural model in which the *B*1 site, with its higher CN, is occupied by a mixture of Zn (or Cd) and Sn atoms, whereas the *B*2 site, with its lower CN, is occupied solely by Zn (or Cd) atoms. A restraint was applied such that the sum of the occupancies over these two sites is unity, but none was placed on the sum of the charges. Furthermore, in the case of $NaCd_{1.5}Sn_{0.5}As_2$, the occupancy of Sn atoms entering the *B*1 site was fixed at exactly 0.25, because Cd and Sn cannot be easily distinguished by their scattering factors. Displacement parameters were kept isotropic for the *B*2 site. Reassuringly, the refinements led to formulas of $NaZn_{1.49(6)}Sn_{0.49(3)}As_2$ and $NaCd_{1.48(1)}Sn_{0.50}As_2$.

The structure determinations for the three remaining quaternary arsenides ($KZn_{1.5}Si_{0.5}As_2$, $KZn_{1.5}Ge_{0.5}As_2$, and $RbZn_{1.5}Ge_{0.5}As_2$) were more straightforward. The tetragonal space group *I*4/*mmm* was chosen and the initial atomic positions found by direct methods were consistent with the $ThCr_2Si_2$-type structure.[21,22] Ternary phases AB_2X_2 adopting this structure type have three sites available to be occupied. The Zn and Si (or Ge) atoms were assumed to disorder over the single available *B* site at 4*d* (0, 1/2, 1/4). As before, because Zn and Si can be distinguished but not Zn and Ge, we allowed the occupancies to vary in the former case (which led to the formula $KZn_{1.47(1)}Si_{0.53(1)}As_2$), but fixed them in the two latter cases. Crystal data and further experimental details are given in Table 2.

In all the treatments above, we have assumed that *Tt* and As atoms do not disorder within the *X* site in either the $CaAl_2Si_2$- or $ThCr_2Si_2$-type structures. However, there have been some precedents in the literature for mixing Si or Ge with As atoms (such as our own earlier work on $Zr(Si_xAs_{1-x})As$ and $Zr(Ge_xAs_{1-x})As$).[23,24] The appropriate candidates for testing the possibility of *Tt*/As disorder are $NaZn_{1.5}Si_{0.5}As_2$ and $KZn_{1.5}Sn_{0.5}As_2$ among the $CaAl_2Si_2$-type phases and $KZn_{1.5}Si_{0.5}As_2$ among the $ThCr_2Si_2$-type phases, because the *Tt* and As components provide sufficient contrast in their X-ray scattering and there are no further complications from split sites. Refinements were then performed on models in which *Tt* atoms are allowed to enter *both* the *B* and *X* sites. The occupancies converged to the following values for the *B* and *X* sites, respectively: 0.71(1) Zn/0.29(3) Si and 0.03(3) Si/0.97(3) As for $NaZn_{1.5}Si_{0.5}As_2$; 0.75(1) Zn/0.25(1) Sn and 0.02(1) Sn/0.98(1) As for $KZn_{1.5}Sn_{0.5}As_2$; 0.75(1) Zn/0.25(1) Si and 0.00(1) Si/1.00(1) As for $KZn_{1.5}Si_{0.5}As_2$. These results provide convincing evidence that the *X* site is essentially occupied only by As atoms, and we extrapolate this conclusion to all members of the quaternary arsenides $AM_{1.5}Tt_{0.5}As_2$.

Atomic positions were standardized with the program *STRUCTURE TIDY*.[25] Final values of the positional and displacement parameters are given in Tables 3 and 4, and selected interatomic distances are listed in Tables 5 and 6. Further data, in the form of crystallographic information files (CIFs), are available as Supporting Information or may be obtained from Fachinformationszentrum Karlsruhe, Abt. PROKA, 76344 Eggenstein-Leopoldshafen, Germany (No. CSD-425474 to 425483).

Band Structure Calculations. Tight-binding linear muffin tin orbital band structure calculations were performed within the local density and atomic spheres approximation with use of the Stuttgart TB-LMTO-ASA program (version 4.7).[26] The basis sets included Na 3s/3p/3d, K 4s/4p/3d, Zn 4s/4p/3d, Cd 5s/5p/4d/4f, Si 3s/3p/3d, Ge 4s/4p/4d, Sn 5s/5p/5d/4f, and As 4s/4p/4d orbitals, with the Na 3p/3d, K 4p/3d, Cd 4f, Si 3d, Ge 4d, Sn 5d/4f, and As 4d orbitals being downfolded. Integrations in reciprocal space were carried out with an improved tetrahedron method over 131 irreducible *k* points within the first Brillouin zone for $CaAl_2Si_2$-type superstructures, as described below.

Because the arsenides $AM_{1.5}Tt_{0.5}As_2$ exhibit site disorder of the *M* and *Tt* atoms, it was necessary to develop ordered model structures for these calculations. For both $CaAl_2Si_2$- and $ThCr_2Si_2$-type structures, the 0.25 *Tt* occupancy could be modeled by distributing *Tt* atoms in an ordered fashion in (i) half of the *B* sites within every other slab of

dx.doi.org/10.1021/ic302627n | *Inorg. Chem.* 2013, 52, 3148−3158

Table 1. Crystallographic Data for $AM_{1.5}Tt_{0.5}As_2$ Compounds with $CaAl_2Si_2$-Type Structure

formula	$NaZn_{1.47(2)}Si_{0.53(2)}As_2$	$NaZn_{1.50}Ge_{0.50}As_2$	$NaZn_{1.49(6)}Sn_{0.49(3)}As_2$	$NaCd_{1.48(1)}Sn_{0.50}As_2$
formula mass (amu)	284.93	307.18	330.23	400.77
space group	$P\bar{3}m1$ (No. 164)	$P\bar{3}m1$ (No. 164)	$P\bar{3}m1$ (No. 164)	$P\bar{3}m1$ (No. 164)
a (Å)	4.0662(3)	4.0948(3)	4.1637(2)	4.3726(2)
c (Å)	7.4120(5)	7.4463(5)	7.5090(4)	7.4647(4)
V (Å^3)	106.13(1)	108.13(1)	112.74(1)	123.60(1)
Z	1	1	1	1
ρ_{calcd} (g cm^{-3})	4.458	4.717	4.864	5.384
T (K)	173(2)	173(2)	173(2)	173(2)
crystal dimensions (mm)	0.04 × 0.06 × 0.12	0.03 × 0.20 × 0.20	0.05 × 0.08 × 0.10	0.08 × 0.13 × 0.14
radiation	graphite monochromated Mo Kα, λ = 0.71073 Å			
μ(Mo Kα) (mm^{-1})	24.03	26.85	25.19	22.15
transmission factors	0.178–0.494	0.066–0.520	0.198–0.419	0.130–0.291
2θ limits	5.50–66.00°	5.48–66.18°	5.42–66.28°	5.46–66.18°
data collected	$-6 \le h \le 6$, $-6 \le k \le 6$, $-11 \le l \le 11$	$-6 \le h \le 6$, $-6 \le k \le 6$, $-11 \le l \le 11$	$-6 \le h \le 6$, $-6 \le k \le 6$, $-11 \le l \le 11$	$-6 \le h \le 6$, $-6 \le k \le 6$, $-11 \le l \le 11$
no. of data collected	1473	1488	1571	1724
no. of unique data, including $F_o^2 < 0$	189 (R_{int} = 0.027)	191 (R_{int} = 0.025)	198 (R_{int} = 0.020)	215 (R_{int} = 0.009)
no. of unique data, with $F_o^2 > 2\sigma(F_o^2)$	183	187	190	211
no. of variables	11	10	15	14
$R(F)$ for $F_o^2 > 2\sigma(F_o^2)$[a]	0.023	0.032	0.014	0.024
$R_w(F_o^2)$[b]	0.048	0.085	0.034	0.060
goodness of fit	1.20	1.35	1.16	1.27
$(\Delta\rho)_{max}$, $(\Delta\rho)_{min}$ (e Å^{-3})	1.88, −2.03	2.09, −2.68	0.55, −0.87	1.01, −2.21
formula	$KZn_{1.54(1)}Sn_{0.46(1)}As_2$	$KCd_{1.50}Sn_{0.50}As_2$	$RbCd_{1.50}Sn_{0.50}As_2$	
formula mass (amu)	346.34	416.89	463.26	
space group	$P\bar{3}m1$ (No. 164)	$P\bar{3}m1$ (No. 164)	$P\bar{3}m1$ (No. 164)	
a (Å)	4.1985(5)	4.4174(3)	4.4263(7)	
c (Å)	8.1471(9)	8.1638(5)	8.4586(14)	
V (Å^3)	124.37(3)	137.96(2)	143.52(4)	
Z	1	1	1	
ρ_{calcd} (g cm^{-3})	4.624	5.018	5.360	
T (K)	173(2)	173(2)	173(2)	
crystal dimensions (mm)	0.07 × 0.14 × 0.16	0.04 × 0.10 × 0.10	0.04 × 0.04 × 0.12	
radiation	graphite monochromated Mo Kα, λ = 0.71073 Å			
μ(Mo Kα) (mm^{-1})	23.59	20.52	27.43	
transmission factors	0.106–0.348	0.254–0.514	0.200–0.491	
2θ limits	5.00–66.18°	4.98–66.26°	4.82–65.86°	
data collected	$-6 \le h \le 6$, $-6 \le k \le 6$, $-12 \le l \le 12$	$-6 \le h \le 6$, $-6 \le k \le 6$, $-12 \le l \le 12$	$-6 \le h \le 6$, $-6 \le k \le 6$, $-12 \le l \le 12$	
no. of data collected	1776	1966	2034	
no. of unique data, including $F_o^2 < 0$	219 (R_{int} = 0.019)	236 (R_{int} = 0.017)	246 (R_{int} = 0.014)	

dx.doi.org/10.1021/ic302627n | Inorg. Chem. 2013, 52, 3148–3158

Table 1. continued

no. of unique data, with $F_o^2 > 2\sigma(F_o^2)$	216	230	242	
no. of variables	12	10	10	
$R(F)$ for $F_o^2 > 2\sigma(F_o^2)$[a]	0.013	0.018	0.023	
$R_w(F_o^2)$[b]	0.032	0.044	0.061	
goodness of fit	1.17	1.22	1.19	
$(\Delta\rho)_{max}$, $(\Delta\rho)_{min}$ (e Å^{-3})	1.76, −0.78	1.72, −2.45	3.63, −1.75	

[a] $R(F) = \sum||F_o| - |F_c||/\sum|F_o|$. [b] $R_w(F_o^2) = [\sum[w(F_o^2 - F_c^2)^2]/\sum wF_o^4]^{1/2}$; $w^{-1} = [\sigma^2(F_o^2) + (Ap)^2 + Bp]$, where $p = [\max(F_o^2,0) + 2F_c^2]/3$.

edge-sharing tetrahedra, or (ii) a quarter of the *B* sites within every slab (Figure S3 in Supporting Information). The latter was found to be more stable than the former by 0.48 eV/f.u. for $NaZn_{1.5}Si_{0.5}As_2$ ($CaAl_2Si_2$-type) and by 0.18 eV/f.u. for $KZn_{1.5}Si_{0.5}As_2$ ($ThCr_2Si_2$-type). Thus, subsequent calculations were made on this type of site distribution ($CaAl_2Si_2$-type in space group $P\bar{3}m1$ with a $2\boldsymbol{a} \times 2\boldsymbol{b} \times \boldsymbol{c}$ superstructure, or $ThCr_2Si_2$-type in space group $P4_2/mcm$ with a $\sqrt{2}\boldsymbol{a} \times \sqrt{2}\boldsymbol{b} \times \boldsymbol{c}$ superstructure). To gauge the reliability of these calculations, the $ThCr_2Si_2$-type superstructure model for $KZn_{1.5}Si_{0.5}As_2$ was optimized by varying the c'/a' ($= c/(\sqrt{2}a)$) ratio and the *z*-coordinate of the As atom, while the cell volume was kept constant, and identifying the total energy minima. The resulting cell parameters and bond distances in the optimized structure were within 2% of the observed values. In view of this good agreement, calculations on other compounds were made using cell and positional parameters taken from the experimentally determined crystal structures. Further details of these calculations are provided in the context of the discussion of the results.

RESULTS AND DISCUSSION

Crystal Structures. Within the series of quaternary arsenides $AM_{1.5}Tt_{0.5}As_2$ (A = Na, K, Rb; M = Zn, Cd; Tt = Si, Ge, Sn), 10 compounds out of the 18 possible permutations could be prepared by stoichiometric reactions of the elements at 650 °C (Na and K samples) or 600 °C (Rb samples). Seven of them adopt the trigonal $CaAl_2Si_2$-type structure (space group $P\bar{3}m1$),[20] and the remaining three adopt the tetragonal $ThCr_2Si_2$-type structure (space group $I4/mmm$),[21,22] both commonly found for AB_2X_2 phases (Tables 1 and 2). In either structure, only one main crystallographic site is available for each of the *A*, *B*, and *X* atoms. The *B* site is thus occupied by a disordered mixture of 75% *M* and 25% *Tt* atoms (Tables 3 and 4).

Both structures are generated by a stacking along the *c*-direction of $[B_2As_2]$ slabs (B = 0.75 M + 0.25 Tt), built up of edge-sharing BAs_4 tetrahedra and interleaved with nets of the *A* cations (Figure 1). The structure of the $CaAl_2Si_2$-type compounds can also be described as consisting of an arrangement of hexagonal nets of As atoms (in hcp stacking sequence **AB**), with half the octahedral interstices filled by *A* atoms and half the tetrahedral interstices by *B* atoms. The $[B_2As_2]$ slabs thus contain both up- and down-pointing BAs_4 tetrahedra with their 3-fold rotation axes aligned parallel to *c*. Correspondingly, the structure of the $ThCr_2Si_2$-type compounds could be viewed as an arrangement of square nets of As atoms, but in a stacking sequence **ABBA**. The *B* atoms occupy tetrahedral interstices within **AB** pairs of nets to form the $[B_2As_2]$ slabs in which BAs_4 tetrahedra are aligned with their 4-fold improper rotation axes ($\bar{4}$) parallel to *c*, and the *A* atoms occupy square prismatic (nearly cubic) interstices within **AA** (or **BB**) pairs of nets.

On proceeding from the $CaAl_2Si_2$- to the $ThCr_2Si_2$-type structure, the increase in coordination number (CN) of the *A* atom from 6 to 8 is consistent with the tendency of the former structure to form with the smaller alkali metals (Na- and K-containing members) and the latter with the larger alkali metals (K- and Rb-containing members). The higher CN is also accompanied by an expansion of *A*−As distances, as seen by comparing the K−As distances in $KZn_{1.5}Sn_{0.5}As_2$ ($CaAl_2Si_2$-type, 3.3571(4) Å) vs $KZn_{1.5}Si_{0.5}As_2$ ($ThCr_2Si_2$-type, 3.5400(7) Å), or the Rb−As distances in $RbCd_{1.5}Sn_{0.5}As_2$ ($CaAl_2Si_2$-type, 3.4982(7) Å) vs $RbZn_{1.5}Ge_{0.5}As_2$ ($ThCr_2Si_2$-type, 3.6228(6) Å), for example. Whereas the *A*−As distances are unextraordinary, the *B*−As distances within the BAs_4 tetrahedral groups deserve

dx.doi.org/10.1021/ic302627n | Inorg. Chem. 2013, 52, 3148−3158

Table 2. Crystallographic Data for $AM_{1.5}Tt_{0.5}As_2$ Compounds with $ThCr_2Si_2$-Type Structure

formula	$KZn_{1.47(1)}Si_{0.53(1)}As_2$	$KZn_{1.50}Ge_{0.50}As_2$	$RbZn_{1.50}Ge_{0.50}As_2$
formula mass (amu)	301.04	323.29	369.66
space group	*I*4/*mmm* (No. 139)	*I*4/*mmm* (No. 139)	*I*4/*mmm* (No. 139)
a (Å)	4.0613(10)	4.0872(4)	4.1157(5)
c (Å)	14.258(3)	14.312(2)	14.662(2)
V (Å^3)	235.18(10)	239.08(4)	248.36(5)
Z	2	2	2
ρ_{calcd} (g cm^{-3})	4.251	4.491	4.943
T (K)	173(2)	173(2)	173(2)
crystal dimensions (mm)	0.04 × 0.04 × 0.15	0.03 × 0.08 × 0.10	0.02 × 0.09 × 0.11
radiation	graphite monochromated Mo Kα, λ = 0.71073 Å		
μ(Mo Kα) (mm^{-1})	22.48	25.07	33.03
transmission factors	0.137–0.558	0.191–0.634	0.113–0.526
2θ limits	5.72–66.50°	5.70–66.22°	5.56–66.50°
data collected	$-6 \le h \le 6, -6 \le k \le 6, -21 \le l \le 22$	$-6 \le h \le 6, -6 \le k \le 6, -22 \le l \le 22$	$-6 \le h \le 6, -6 \le k \le 6, -22 \le l \le 22$
no. of data collected	1639	1691	1744
no. of unique data, including $F_o^2 < 0$	171 (R_{int} = 0.019)	171 (R_{int} = 0.019)	176 (R_{int} = 0.030)
no. of unique data, with $F_o^2 > 2\sigma(F_o^2)$	158	160	161
no. of variables	10	9	9
$R(F)$ for $F_o^2 > 2\sigma(F_o^2)^a$	0.015	0.020	0.022
$R_w(F_o^2)^b$	0.034	0.038	0.043
goodness of fit	1.18	1.18	1.10
$(\Delta\rho)_{max}$, $(\Delta\rho)_{min}$ (e Å^{-3})	1.05, −0.72	1.23, −1.08	1.61, −1.63

$^aR(F) = \sum||F_o| - |F_c||/\sum|F_o|$. $^bR_w(F_o^2) = [\sum[w(F_o^2 - F_c^2)^2]/\sum wF_o^4]^{1/2}$; $w^{-1} = [\sigma^2(F_o^2) + (Ap)^2 + Bp]$, where $p = [\max(F_o^2,0) + 2F_c^2]/3$.

closer examination given the disorder of different *M* and *Tt* atoms that occurs within the *B* site. In general, the *B*–As distances (Tables 5 and 6) agree well with literature values for compounds containing similar BAs_4 tetrahedra (e.g., Zn–As, 2.5629(7) Å in $LaZn_{0.66}As_2$;[27] Cd–As, 2.547(9)–2.752(2) Å in $LaCd_3As_3$;[28] Si–As, 2.351(1)–2.441(1) Å in Na_5SiAs_3;[29] Ge–As, 2.433(1)–2.520(1) Å in Na_5GeAs_3;[30] Sn–As, 2.630(1)–2.712(1) Å in K_5SnAs_3[31]) and can be compared with the sum of Pauling metallic radii (R_1) (Zn–As, 2.42 Å; Cd–As, 2.59 Å; Si–As, 2.38 Å; Ge–As, 2.45 Å; Sn–As 2.63 Å).[32] Among the possible combinations of *M* and *Tt* atoms, all but Cd–Si and Cd–Ge are observed, which is not unexpected considering the disparate atomic sizes within these pairs of elements. However, the formation of compounds with the Zn–Sn combination is a little surprising. Of course, this analysis of distances neglects the charge transfer that would take place to modify the sizes of atoms within the solid. It is interesting to note that two of the compounds, $NaZn_{1.5}Sn_{0.5}As_2$ and $NaCd_{1.5}Sn_{0.5}As_2$, exhibit a minor site, with trigonal planar (CN3) coordination, split off from the main tetrahedrally coordinated *B* site (Figure S4 in Supporting Information). Occupation of this site at a low level (<11%) by the smaller Zn or, to a lesser extent, Cd atoms perhaps reflects the preference to recover shorter distances that are more suitable for these atoms.

With the *X* component fixed to be As within the AB_2X_2 compounds of $CaAl_2Si_2$-type, it is possible to examine structural trends more closely as a function of the *A* or *B* component. Figure 2 shows plots of the *c*/*a* ratio as the *A* component is changed in $ACd_{1.5}Sn_{0.5}As_2$ and as the *B* component is changed in $NaM_{1.5}Tt_{0.5}As_2$. The *c*/*a* ratio is a measure of the expansion or compression of the structure along the *c* axis. In turn, this is caused by distortions of the coordination polyhedra around the *A* or *B* atoms, as expressed by the bond angles η (∠As–*A*–As) and ε (∠As–*B*–As), according to the notation established by Klüfers and Mewis.[3] In the series $ACd_{1.5}Sn_{0.5}As_2$, the *B* component (mixture of Cd and Sn atoms) is fixed while the *A* component is varied (*A* = Na, K, Rb). Substitution with a larger alkali metal on progressing from $NaCd_{1.5}Sn_{0.5}As_2$ to $RbCd_{1.5}Sn_{0.5}As_2$ leads to an expansion along *c*, caused primarily by the elongation of the AAs_6 octahedra along the 3-fold rotation axes parallel to *c* (Figure 2a). The As–*A*–As bond angle deviates away from the ideal value of 90° and becomes more acute (from 88° to 78°) to accommodate longer *A*–As distances, while respecting the need to maintain constant *B*–As distances of ∼2.7 Å within the $[Cd_{1.5}Sn_{0.5}As_2]$ slabs. In the series $NaM_{1.5}Tt_{0.5}As_2$, the *A* component is fixed while the *B* component (mixture of *M* and *Tt* atoms) is varied (*B* = Zn–Si, Zn–Ge, Zn–Sn, Cd–Sn). Substitution with a set of larger *M* and *Tt* atoms on progressing from $NaZn_{1.5}Si_{0.5}As_2$ to $NaCd_{1.5}Sn_{0.5}As_2$ leads to a compression along *c* (Figure 2b). Interestingly, the dominant cause for this compression is still the identity of the *A* component, for which the As–Na–As angles gradually increase (from 82° to 88°), while the geometry around the *B* component reaches a limit in which the As–*B*–As angles do not decrease below 110°. These observations are consistent with the expectation that the geometric requirements for $CaAl_2Si_2$-type phases AB_2X_2 will be more rigid within the $[B_2X_2]$ slab because of the directional character of covalent *B*–*X* bonds, in contrast to the greater flexibility allowed around the *A* atoms which participate in more ionic *A*–*X* bonds.

A structure map has been previously developed to define the limits of stability of the $CaAl_2Si_2$-type structure for ternary AB_2X_2 phases, on the basis of the average principal quantum number $\bar{n}$ and a parameter *f* that is a weighted function of Slater atomic radii for *A*, *B*, and *X* ($f = r_A/(r_B + 0.2r_X)$).[3] To establish a similar structure map applicable for the quaternary arsenides $AM_{1.5}Tt_{0.5}As_2$, it will be important to introduce the radius ratio r_M/r_{Tt} to take into account the relative sizes of *M* and *Tt* atoms disordered over the *B* site, with the expectation that the structure will not be stable if these atoms are too disparate in

dx.doi.org/10.1021/ic302627n | Inorg. Chem. 2013, 52, 3148–3158

Table 3. Atomic Coordinates and Equivalent Isotropic Displacement Parameters for $AM_{1.5}Tt_{0.5}As_2$ Compounds with $CaAl_2Si_2$-Type Structure

atom	Wyckoff position	occupancy	x	y	z	U_{eq} (Å^2)[a]
		$NaZn_{1.47(2)}Si_{0.53(2)}As_2$				
Na	1*a*	1	0	0	0	0.0207(8)
B	2*d*	0.733(8) Zn, 0.267(8) Si	1/3	2/3	0.6294(1)	0.0182(3)
As	2*d*	1	1/3	2/3	0.27155(9)	0.0187(3)
		$NaZn_{1.50}Ge_{0.50}As_2$				
Na	1*a*	1	0	0	0	0.0202(11)
B	2*d*	0.75 Zn, 0.25 Ge	1/3	2/3	0.6287(2)	0.0199(4)
As	2*d*	1	1/3	2/3	0.2689(1)	0.0150(4)
		$NaZn_{1.49(6)}Sn_{0.49(3)}As_2$				
Na	1*a*	1	0	0	0	0.0228(4)
*B*1	2*d*	0.64(3) Zn, 0.24(2) Sn	1/3	2/3	0.6286(1)	0.0171(2)
*B*2	2*d*	0.106(4) Zn	1/3	2/3	0.704(1)	0.012(1)
As	2*d*	1	1/3	2/3	0.26329(4)	0.0135(2)
		$NaCd_{1.48(1)}Sn_{0.50}As_2$				
Na	1*a*	1	0	0	0	0.0253(9)
*B*1	2*d*	0.692(5) Cd, 0.25 Sn	1/3	2/3	0.6358(1)	0.0212(3)
*B*2	2*d*	0.050(4) Cd	1/3	2/3	0.721(2)	0.021(3)
As	2*d*	1	1/3	2/3	0.25018(9)	0.0188(3)
		$KZn_{1.54(1)}Sn_{0.46(1)}As_2$				
K	1*a*	1	0	0	0	0.0170(2)
B	2*d*	0.769(6) Zn, 0.232(6) Sn	1/3	2/3	0.62324(5)	0.0154(2)
As	2*d*	1	1/3	2/3	0.28507(5)	0.0133(1)
		$KCd_{1.50}Sn_{0.50}As_2$				
K	1*a*	1	0	0	0	0.0172(3)
B	2*d*	0.75 Cd, 0.25 Sn	1/3	2/3	0.62761(6)	0.0169(2)
As	2*d*	1	1/3	2/3	0.27332(9)	0.0164(2)
		$RbCd_{1.50}Sn_{0.50}As_2$				
Rb	1*a*	1	0	0	0	0.0159(3)
B	2*d*	0.75 Cd, 0.25 Sn	1/3	2/3	0.62313(6)	0.0154(2)
As	2*d*	1	1/3	2/3	0.2824(1)	0.0155(3)

[a] U_{eq} is defined as one-third of the trace of the orthogonalized U_{ij} tensor.

size. Because the *X* component is fixed to be As in these quaternary arsenides but the *B* component contains two types of atoms, we omit consideration of the radius of the *X* atom and replace the parameter *f* by the radius ratio r_A/r_B where r_B is the weighted average of the *M* and *Tt* radii. We have also opted to use Pauling metallic radii (R_1)[32] instead of Slater atomic radii,[33] although either set will probably do. A plot of these two radius ratios is sufficient to reveal a good demarcation of those compounds that adopt the $CaAl_2Si_2$-type vs $ThCr_2Si_2$-type structures, as well as those that do not form (Figure 3). Inspection of this plot confirms that smaller alkali-metal atoms that occupy the *A* site favor the $CaAl_2Si_2$-type structure (with CN6 for *A*). When larger alkali-metal atoms are present so that r_A/r_B exceeds 1.6, the $ThCr_2Si_2$-type structure becomes preferred because the *A* site now has CN8. The nonexistent compound $RbZn_{1.5}Si_{0.5}As_2$ lies at the highest r_A/r_B point of 1.8, which represents the limiting value beyond which even the $ThCr_2Si_2$-type structure does not form within this series of quaternary arsenides. For both structure types, r_M/r_{Tt} does not generally stray far from 1.0 except for the unexpected formation

Table 4. Atomic Coordinates and Equivalent Isotropic Displacement Parameters for $AM_{1.5}Tt_{0.5}As_2$ Compounds with $ThCr_2Si_2$-Type Structure

atom	Wyckoff position	occupancy	x	y	z	U_{eq} (Å^2)[a]
		$KZn_{1.47(1)}Si_{0.53(1)}As_2$				
K	2*a*	1	0	0	0	0.0217(3)
B	4*d*	0.736(5) Zn, 0.264(5) Si	0	1/2	1/4	0.0215(2)
As	4*e*	1	0	0	0.35483(3)	0.0237(2)
		$KZn_{1.50}Ge_{0.50}As_2$				
K	2*a*	1	0	0	0	0.0205(4)
B	4*d*	0.75 Zn, 0.25 Ge	0	1/2	1/4	0.0244(2)
As	4*e*	1	0	0	0.35629(4)	0.0197(2)
		$RbZn_{1.50}Ge_{0.50}As_2$				
Rb	2*a*	1	0	0	0	0.0188(3)
B	4*d*	0.75 Zn, 0.25 Ge	0	1/2	1/4	0.0241(3)
As	4*e*	1	0	0	0.35284(6)	0.0192(2)

[a] U_{eq} is defined as one-third of the trace of the orthogonalized U_{ij} tensor.

Table 5. Interatomic Distances (Å) in $AM_{1.5}Tt_{0.5}As_2$ Compounds with $CaAl_2Si_2$-Type Structure[a]

	$NaZn_{1.47(2)}Si_{0.53(2)}As_2$	$NaZn_{1.50}Ge_{0.50}As_2$
A–As (× 6)	3.0923(5)	3.0980(6)
A–*B* (× 6)	3.6133(7)	3.6378(9)
B–As (× 3)	2.4597(4)	2.4842(5)
B–As	2.6524(12)	2.6793(14)
B–*B* (× 3)	3.0317(12)	3.0434(14)
	$NaZn_{1.49(6)}Sn_{0.49(3)}As_2$	$NaCd_{1.48(1)}Sn_{0.50}As_2$
A–As (× 6)	3.1125(2)	3.1402(4)
A–*B*1 (× 6)/ *A*–*B*2 (× 6)	3.6817(7)/3.273(5)	3.7103(6)/3.272(10)
*B*1–As (× 3)/ *B*2–As (× 3)	2.5372(3)/2.4162(7)	2.6643(3)/2.5336(14)
*B*1–As	2.7433(9)	2.8781(10)
*B*1–*B*1 (× 3)	3.0839(11)	3.2373(10)
	$KZn_{1.54(1)}Sn_{0.46(1)}As_2$	$KCd_{1.50}Sn_{0.50}As_2$
A–As (× 6)	3.3571(4)	3.3887(5)
A–*B* (× 6)	3.9112(4)	3.9682(4)
B–As (× 3)	2.5365(3)	2.6756(3)
B–As	2.7551(6)	2.8924(9)
B–*B* (× 3)	3.1478(6)	3.2933(6)
	$RbCd_{1.50}Sn_{0.50}As_2$	
A–As (× 6)	3.4982(7)	
A–*B* (× 6)	4.0857(6)	
B–As (× 3)	2.6775(5)	
B–As	2.8819(11)	
B–*B* (× 3)	3.2969(8)	

[a] Site *B* is occupied by a mixture of *M* (Zn or Cd) and *Tt* (Si, Ge, or Sn) atoms.

Table 6. Interatomic Distances (Å) in $AM_{1.5}Tt_{0.5}As_2$ Compounds with $ThCr_2Si_2$-Type Structure[a]

	$KZn_{1.47(1)}Si_{0.53(1)}As_2$	$KZn_{1.50}Ge_{0.50}As_2$	$RbZn_{1.50}Ge_{0.50}As_2$
A–As (× 8)	3.5400(7)	3.5472(5)	3.6228(6)
A–*A* (× 4)	4.0613(10)	4.0872(4)	4.1157(5)
B–As (× 4)	2.5214(5)	2.5476(4)	2.5512(5)
B–*B* (× 4)	2.8718(7)	2.8901(3)	2.9102(4)

[a] Site *B* is occupied by a mixture of *M* (Zn) and *Tt* (Si or Ge) atoms.

dx.doi.org/10.1021/ic302627n | Inorg. Chem. 2013, 52, 3148–3158

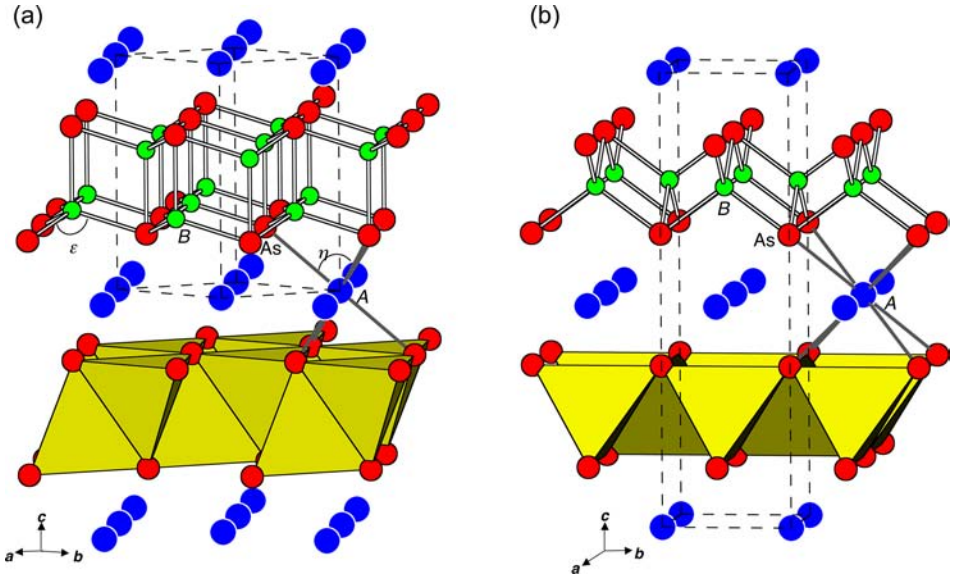

Figure 1. (a) $CaAl_2Si_2$-type or (b) $ThCr_2Si_2$-type structures of quaternary arsenides $AM_{1.5}Tt_{0.5}As_2$ (A = Na, K, Rb; M = Zn, Cd; Tt = Si, Ge, Sn), with the slabs of edge-sharing BAs_4 tetrahedra (B = 0.75 M and 0.25 Tt) and the coordination of A atoms highlighted. In (a), the bond angles around the A atom (η = ∠As−A−As) and the B atom (ε = ∠As−B−As) are defined as shown.

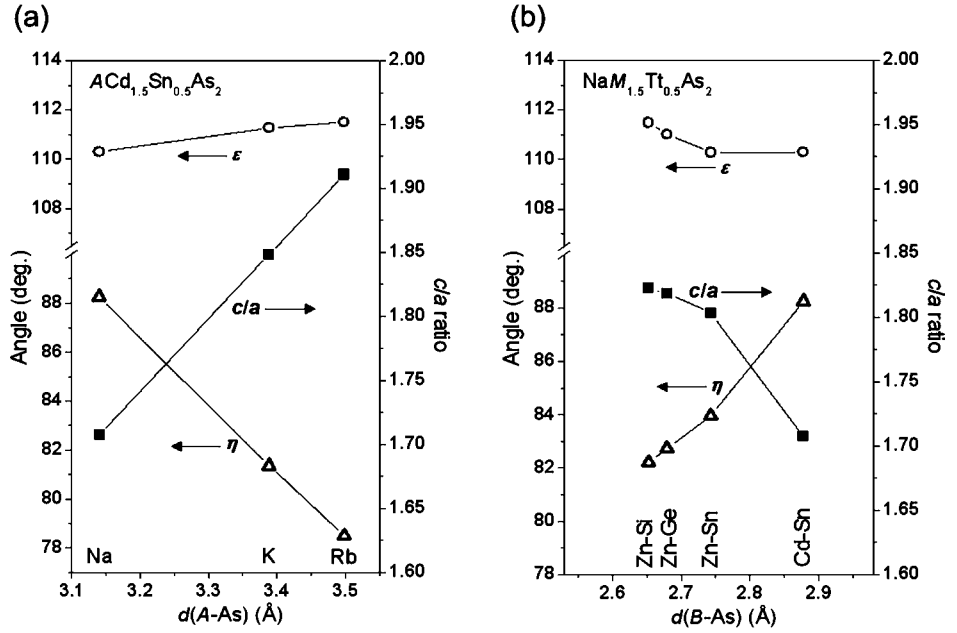

Figure 2. Plots of c/a ratio and bond angles (around A atoms (η) and B atoms (ε), as defined in Figure 1) for two series of $CaAl_2Si_2$-type phases: (a) $ACd_{1.5}Sn_{0.5}As_2$ (A = Na, K, Rb) and (b) $NaM_{1.5}Tt_{0.5}As_2$ (B = 0.75 M and 0.25 Tt, with Zn−Si, Zn−Ge, Zn−Sn, Cd−Sn combinations).

of $NaZn_{1.5}Sn_{0.5}As_2$ and $KZn_{1.5}Sn_{0.5}As_2$ noted earlier. This anomaly might be rectified through use of Slater atomic radii, according to which Zn and Sn have more similar radii (r_M/r_{Tt} = 0.93) than in the case of Pauling metallic radii (r_M/r_{Tt} = 0.84).[32,33] The drawback of this choice is that the radius ratio then becomes too large for the Zn−Si combination (r_M/r_{Tt} = 1.23). In any event, this analysis neglects the charge transfer that would be expected to occur from the electropositive to electronegative components, so that in the ionic extreme, the nominal charges would be Zn^{2+} and Sn^{4+} and their radii would be modified from those of the neutral atoms. $RbZn_{1.5}Sn_{0.5}As_2$ is a potential $CaAl_2Si_2$-type phase but it lies at the boundaries of low r_M/r_{Tt} and high r_A/r_B values; its nonexistence may be attributed to significant distortions that would take place around the Rb atoms, giving extremely acute η angles, which are already at 77.41(1)° in $KZn_{1.5}Sn_{0.5}As_2$.

Electronic Structure and Bonding. The charge-balanced formulation $(A^+)(M^{2+})_{1.5}(Tt^{4+})_{0.5}(As^{3-})_2$, obtained in the extreme picture of ionic bonding when the Zintl concept is applied, corresponds to closed-shell electron configurations for all atoms. For the $AM_{1.5}Tt_{0.5}As_2$ compounds with the $CaAl_2Si_2$-type structure, the occurrence of fully reduced As atoms implied by this formulation indicates that no As−As bonding takes place. The interslab As−As distances in these compounds are all very long (ranging from 4.661(1) Å in $NaZn_{1.5}Si_{0.5}As_2$ to 5.418(1) Å in $RbCd_{1.5}Sn_{0.5}As_2$). In $ThCr_2Si_2$-type phases, however, it is well-known that anion−anion bonds can potentially form between $[B_2X_2]$ slabs, depending on the

dx.doi.org/10.1021/ic302627n | Inorg. Chem. 2013, 52, 3148−3158

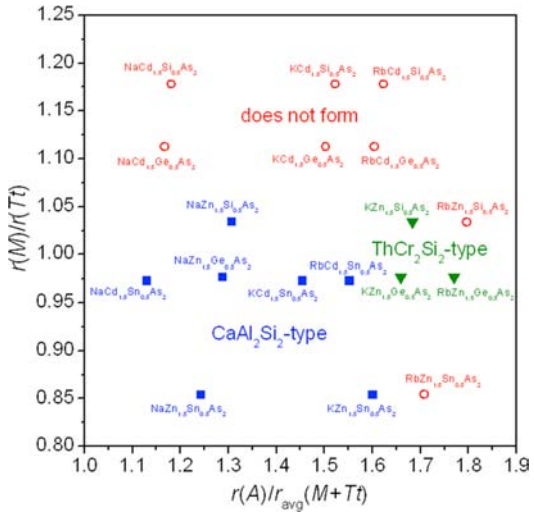

Figure 3. Structure map for quaternary arsenides $AM_{1.5}Tt_{0.5}As_2$ (A = Na, K, Rb; M = Zn, Cd; Tt = Si, Ge, Sn) showing the demarcation of $CaAl_2Si_2$-type structures (blue squares), $ThCr_2Si_2$-type structures (green triangles), and nonexistent members to date (red circles) on the basis of radius ratios.

electron count controlled by the choice of the transition metal component B. This bond formation was first proposed to occur through an internal redox process in which electrons flow back to the transition metal component to alleviate antibonding X–X interactions.[34] Although this elegant explanation has been popular,[35,36] it was later shown to be oversimplified because the position and population of the antibonding X–X levels are intimately linked with intralayer B–B and B–X interactions.[37,38] In particular, the importance of the metal–metal (B–B) interactions has since been corroborated by others.[39−41] For the three $AM_{1.5}Tt_{0.5}As_2$ compounds with the $ThCr_2Si_2$-type structure, the interslab As–As distances are far too long to be bonding (ranging from 4.114(1) Å in $KZn_{1.5}Ge_{0.5}As_2$ to 4.315(1) Å in $RbZn_{1.5}Ge_{0.5}As_2$), as are the intralayer B–B distances (>3.1 Å). Much of the literature of $ThCr_2Si_2$-type phases has focused on examining the effect of d-electron count of the transition metal component, with the A component generally being neglected from consideration or serving a primarily geometric role in separating the $[B_2X_2]$ layers.[5,34,37] However, there is growing recognition that the nature of the A component can strongly influence the physical properties of $ThCr_2Si_2$-type phases,[42,43] and that cation–anion interactions, as well as other factors such as the spin state of the transition metal, are important in determining the adoption of the $CaAl_2Si_2$- vs $ThCr_2Si_2$-type structures, as has been shown for AMn_2P_2 (A = Ca, Sr, Ba).[10,44]

Given the closed-shell configurations of the M^{2+} and Tt^{4+} species, the $AM_{1.5}Tt_{0.5}As_2$ series provides the possibility to isolate the role of the A cation in the adoption of $CaAl_2Si_2$- vs $ThCr_2Si_2$-type structures. This is a challenging problem in which alternative hypothetical structures must be constructed to give reasonable bond lengths. Extended Hückel methods have been previously applied to investigate the stability of isolated $[Mn_2P_2]$ slabs in $CaAl_2Si_2$- and $ThCr_2Si_2$-type structures as a function of band filling, with the assumption that both structures have the same Mn–Mn and Mn–P distances.[5] However, it would be expected that geometrical differences between $CaAl_2Si_2$- and $ThCr_2Si_2$-type polymorphs of a given compound would render these distances to be not identical. Comparison of the observed distances in $AM_{1.5}Tt_{0.5}As_2$ (Tables 5 and 6) reveals trends which we can exploit to define hypothetical model structures. First, on proceeding from $CaAl_2Si_2$- to $ThCr_2Si_2$-type structures, the A–As distances expand in accordance with the change in CN from 6 to 8, close to the difference in Shannon ionic radii for A^+ cations ($\Delta r_{CN6\rightarrow CN8}$ of 0.16 Å for Na^+, 0.13 Å for K^+, and 0.09 Å for Rb^+).[45] Second, although there are two inequivalent sets of B–As distances, typically designated the three shorter lateral "rib" and one longer vertical "handle" bonds,[4] within the BAs_4 tetrahedra in the $CaAl_2Si_2$-type structures, the average B–As distance is retained in the $ThCr_2Si_2$-type structures, all other things being equal. Third, the B–B distances tend to be 0.1–0.2 Å shorter in the $ThCr_2Si_2$-type structures for a fixed combination of M and Tt. We have chosen $KZn_{1.5}Ge_{0.5}As_2$ as a test case in which the $[Zn_{1.5}Ge_{0.5}As_2]$ slabs, containing an ordered distribution of Zn and Ge atoms, were taken from the experimental $ThCr_2Si_2$-type structure and constructed in a hypothetical $CaAl_2Si_2$-type polymorph so as to exhibit differences that are consistent with the changes seen in the rest of the $AM_{1.5}Tt_{0.5}As_2$ series. The $[Zn_{1.5}Ge_{0.5}As_2]$ slabs were then kept invariant while the effect of a change in the alkali-metal component was mimicked by expanding or contracting the structure along the c-direction, which is a good approximation in view of the interpretation of Figure 2a discussed earlier. Plots of the relative total energy determined from LMTO calculations (Figure 4a) confirm that the $ThCr_2Si_2$-type structure is favored at long K–As separations whereas the $CaAl_2Si_2$-type structure is favored at short ones, a result that is consistent, of course, with the coordination preferences of large vs small A cations. Similar calculations were performed on $KCd_{1.5}Sn_{0.5}As_2$ with fixed $[Cd_{1.5}Sn_{0.5}As_2]$ slabs taken from the experimental $CaAl_2Si_2$-type structure and constructed in a hypothetical $ThCr_2Si_2$-type polymorph. The substitution with larger M and Tt atoms increases the in-plane distances so that the $[Cd_{1.5}Sn_{0.5}As_2]$ slabs in $KCd_{1.5}Sn_{0.5}As_2$ are expanded relative to the $[Zn_{1.5}Ge_{0.5}As_2]$ slabs in $KZn_{1.5}Ge_{0.5}As_2$. To compensate for the weakening in K–As interactions accompanying this expansion, it would be expected that the K cations would prefer the lower CN and shorter K–As distances available in the $CaAl_2Si_2$-type structure. Plots of the relative total energy confirm that, at shorter K–As distances, the $ThCr_2Si_2$-type structure becomes highly disfavored, while the $CaAl_2Si_2$-type structure becomes more stable (Figure 4b).

The closed-shell electron configurations in $AM_{1.5}Tt_{0.5}As_2$ also lead to the prediction of semiconducting behavior. Unfortunately, these compounds are moderately air-sensitive, and we have been unable to perform electrical resistivity measurements. There have been many studies of the electrical properties of $ThCr_2Si_2$-type phases, but relatively few on $CaAl_2Si_2$-type phases.[46] The band structure was calculated for one of the $CaAl_2Si_2$-type phases presented here, $NaZn_{1.5}Si_{0.5}As_2$. In fact, the band dispersion diagram reveals that there is no band gap and that the valence and conduction bands overlap slightly (Figure 5a). When the calculations were repeated with the intervening Na^+ cations removed between the $[Zn_{1.5}Si_{0.5}As_2]^-$ slabs, the overlap remains (Figure 5b). These results indicate that the absence of a band gap is intrinsic to the slabs themselves, confirming similar conclusions made previously on other $CaAl_2Si_2$-type phases (including $CaAl_2Si_2$ itself) in which the controlling factor is the difference in electronegativity between the B and X atoms within the $[B_2X_2]$ slabs.[7−10] A lower electronegativity difference leads to greater energy

dx.doi.org/10.1021/ic302627n | Inorg. Chem. 2013, 52, 3148−3158

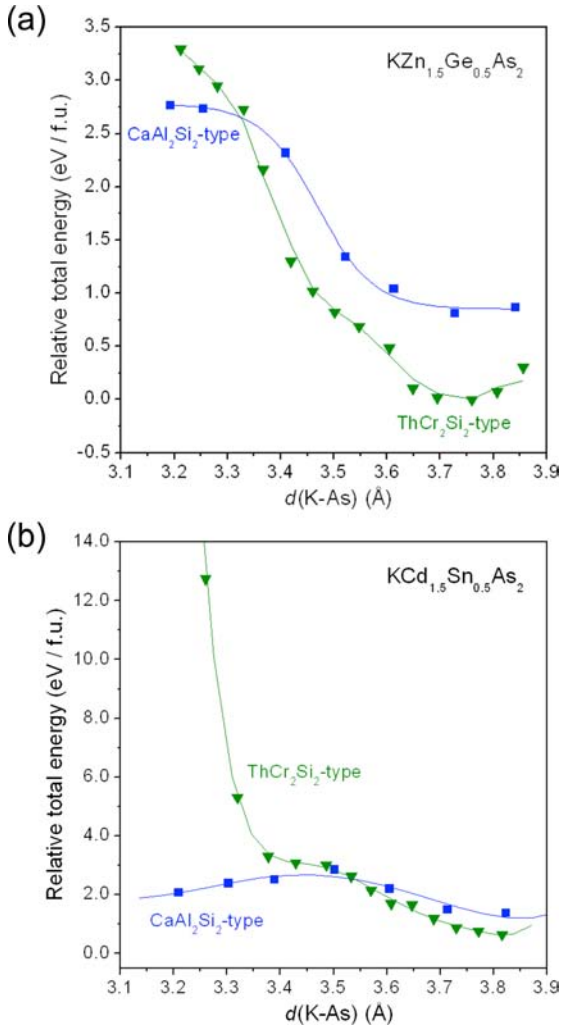

Figure 4. Plots of relative total energy for ordered (a) $KZn_{1.5}Ge_{0.5}As_2$ and (b) $KCd_{1.5}Sn_{0.5}As_2$ models with fixed $[M_{1.5}Tt_{0.5}As_2]$ slabs in $CaAl_2Si_2$- vs $ThCr_2Si_2$-type structures, as a function of K–As distances as the structures are expanded or contracted along the *c*-direction.

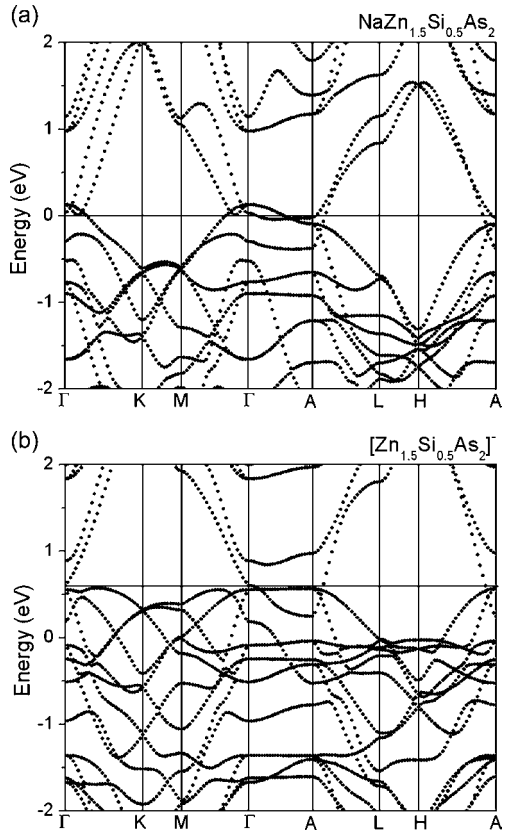

Figure 5. Band dispersion diagrams for ordered models of (a) $NaZn_{1.5}Si_{0.5}As_2$ (with Na atoms included in calculation) and (b) $[Zn_{1.5}Si_{0.5}As_2]^-$ (with Na atoms omitted from calculation).

dispersion of the bands, such that the top of the valence band and the bottom of the conduction band approach each other and eventually overlap. This proposal can be tested within the series $NaZn_{1.5}Si_{0.5}As_2$, $NaZn_{1.5}Ge_{0.5}As_2$, and $NaZn_{1.5}Sn_{0.5}As_2$, which all adopt the $CaAl_2Si_2$-type structure but differ only in the *Tt* component to give $\Delta\chi_{Tt-As}$ = 0.28, 0.17, and 0.22, respectively. The calculated densities of states (DOS) at the Fermi level are 2.0, 3.5, and 0.9 states/eV per cell for $NaZn_{1.5}Si_{0.5}As_2$, $NaZn_{1.5}Ge_{0.5}As_2$, and $NaZn_{1.5}Sn_{0.5}As_2$, respectively. Because the DOS depends on several factors (slopes of bands, number of bands crossed by Fermi level), the agreement is not perfect. However, it is clear that $NaZn_{1.5}Ge_{0.5}As_2$, which corresponds to the combination with the smallest electronegativity difference, gives rise to the greatest overlap of valence and conduction bands.

Implicit in the discussion above is that the *A* cations participate in some degree of covalent bonding, notwithstanding the ionic bonding picture presented in the Zintl formulation. Even though they do not directly influence the electrical properties and provide only small contributions to the DOS at the Fermi level (e.g., 5% for $NaZn_{1.5}Si_{0.5}As_2$ and 8% for $NaZn_{1.5}Ge_{0.5}As_2$), they would be expected to have some orbital interactions with the surrounding As atoms. As shown in the atomic projections of the DOS for $NaZn_{1.5}Si_{0.5}As_2$ (Figure 6a), there is a small mixing of Na 3s with As 4p states primarily in the region from −6 to 0 eV. The mixing leads to weak bonding interactions, as verified by the crystal orbital Hamilton population (COHP) curve (Figure 6b), with an integrated −COHP value (−ICOHP) of 0.14 eV/bond. The sharp spike in the DOS from −8 to −6.5 eV corresponds to the filled 3d band of the Zn atoms. The most important bonding interactions come from mixing of Zn 4s/4p and Si 3s/3p with As 4p states, with all the bonding levels filled just up to the Fermi level. The Zn–As bonds in the three shorter ribs are stronger (−ICOHP of 1.63 eV/bond) than in the longer handle (−ICOHP of 1.18 eV/bond). At the same distances, the Si–As bonds are even stronger (−ICOHP of 2.43 eV/bond for the ribs and 1.84 eV/bond for the handle). When the Na^+ cations are omitted from the calculation, these Zn–As and Si–As bonds are strengthened by 27%, which lends further support to the noninnocent role of these cations. Summed over the unit cell, the contributions to covalent bonding decrease in the order Si–As, Zn–As, and Na–As. Table 7 compares these bonding contributions for the series $NaZn_{1.5}Tt_{0.5}As_2$ (*Tt* = Si, Ge, Sn). Introducing larger *Tt* atoms into the tetrahedral sites necessarily lengthens the Zn–As bonds as well, which gradually become weaker. The observed crystal structure of $NaZn_{1.5}Sn_{0.5}As_2$ reveals that the response to this bond weakening is to relegate a proportion of the smaller Zn atoms to a new split site with trigonal planar coordination (CN3) consistent with more appropriate Zn–As bond lengths.

dx.doi.org/10.1021/ic302627n | *Inorg. Chem.* 2013, 52, 3148–3158

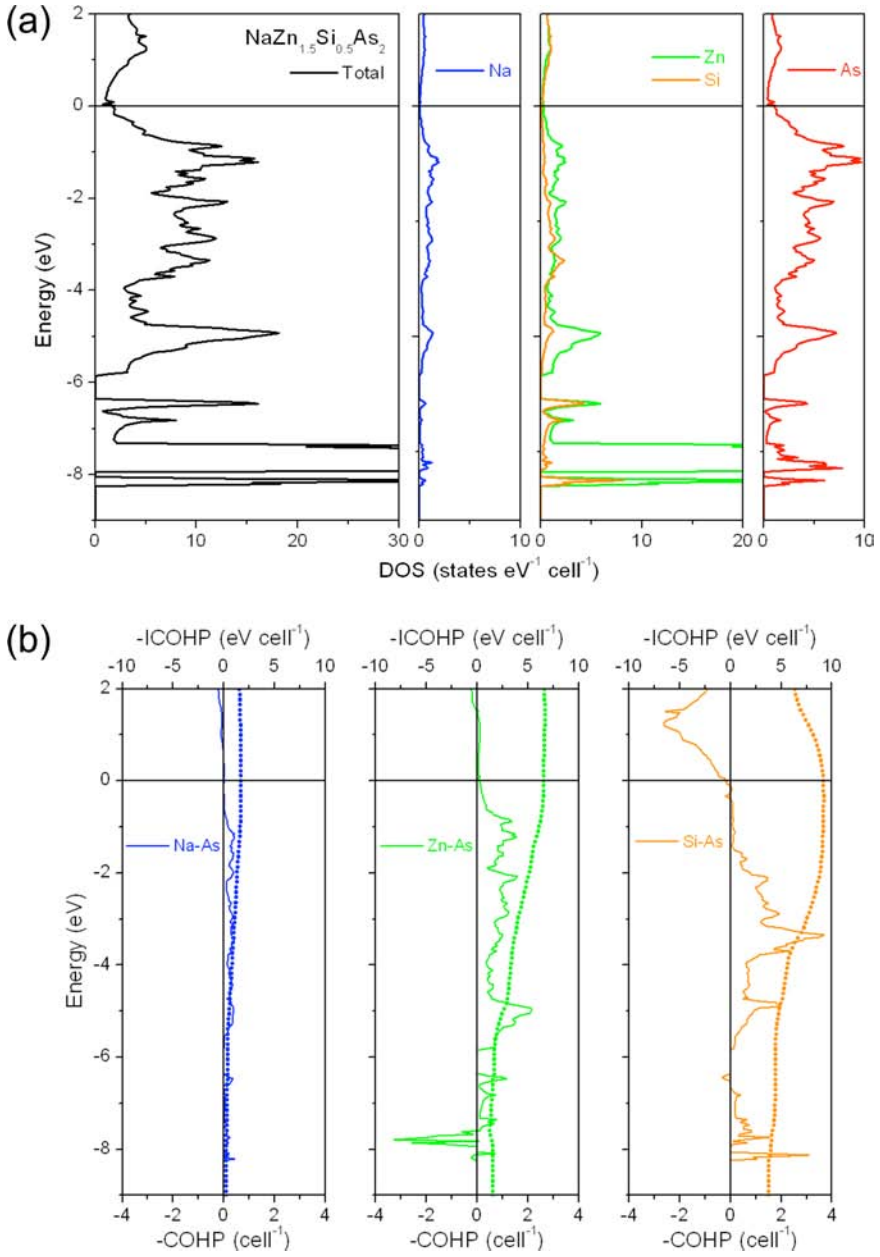

Figure 6. (a) Density of states (DOS) and its atomic projections for $NaZn_{1.5}Si_{0.5}As_2$. (b) Crystal orbital Hamilton population (COHP) curves for Na−As, Zn−As, and Si−As contacts. The Fermi level is at 0 eV.

Table 7. Comparison of −ICOHP Values in $NaZn_{1.5}Tt_{0.5}As_2$ (*Tt* = Si, Ge, Sn)

contact	−ICOHP (eV bond^{-1})	−ICOHP (eV cell^{-1})	contribution (%)
	$NaZn_{1.5}Si_{0.5}As_2$		
Na−As	0.14	1.66	9.6
Zn−As	1.63	6.55	37.7
Si−As	2.28	9.14	52.7
	$NaZn_{1.5}Ge_{0.5}As_2$		
Na−As	0.13	1.53	9.6
Zn−As	1.42	5.70	35.8
Ge−As	2.17	8.70	54.6
	$NaZn_{1.5}Sn_{0.5}As_2$		
Na−As	0.17	2.07	13.0
Zn−As	1.22	4.89	30.8
Sn−As	2.22	8.91	56.1

CONCLUSIONS

Several quaternary arsenides $AM_{1.5}Tt_{0.5}As_2$ with $CaAl_2Si_2$- or $ThCr_2Si_2$-type structures can be prepared in which the combination of *A*, *M*, and *Tt* components satisfies simple radius ratio rules. Because the *M* and *Tt* components necessarily disorder over the same *B* site with tetrahedral coordination, their sizes should not differ greatly and r_M/r_{Tt} is close to 1.0. Consistent with the increase in CN from 6 to 8 for the *A* site, the $CaAl_2Si_2$-type structure is preferred by smaller *A* cations, whereas the $ThCr_2Si_2$-type structure is preferred by larger *A* cations. However, this size preference for the *A* component must be compatible with the geometric requirements of $[M_{1.5}Tt_{0.5}As_2]$ slab, as expressed by the ratio $r_A/r_{avg(M+Tt)}$. It would be interesting to change experimental conditions (e.g., pressure) that might overcome these restrictions to favor the formation of the currently nonexistent

dx.doi.org/10.1021/ic302627n | Inorg. Chem. 2013, 52, 3148−3158

$AM_{1.5}Tt_{0.5}As_2$ members. The electronic structure is largely dominated by these $[M_{1.5}Tt_{0.5}As_2]$ slabs, which can be viewed as relatively rigid and which contain strong covalent bonds, while the *A* cations participate mostly in ionic interactions with these slabs. Band structure calculations confirm that, despite being charge-balanced Zintl phases, these arsenides are predicted to exhibit semimetallic behavior resulting from a small overlap of valence and conduction bands.

■ ASSOCIATED CONTENT

Ⓢ Supporting Information

X-ray crystallographic files in CIF format, EDX analyses, powder XRD patterns, SEM images, and additional figures of structures. This material is available free of charge via the Internet at http://pubs.acs.org.

■ AUTHOR INFORMATION

Corresponding Author

*E-mail: arthur.mar@ualberta.ca.

Notes

The authors declare no competing financial interest.

■ ACKNOWLEDGMENTS

This work was supported by the Natural Sciences and Engineering Research Council of Canada.

■ REFERENCES

(1) Villars, P.; Cenzual, K. *Pearson's Crystal Data – Crystal Structure Database for Inorganic Compounds*, release 2010/11; ASM International, Materials Park, OH, 2010.
(2) Mandrus, D.; Sefat, A. S.; McGuire, M. A.; Sales, B. C. *Chem. Mater.* **2010**, *22*, 715–723.
(3) Klüfers, P.; Mewis, A. *Z. Kristallogr.* **1984**, *169*, 135–147.
(4) Zheng, C.; Hoffmann, R.; Nesper, R.; von Schnering, H.-G. *J. Am. Chem. Soc.* **1986**, *108*, 1876–1884.
(5) Zheng, C.; Hoffmann, R. *J. Solid State Chem.* **1988**, *72*, 58–71.
(6) Burdett, J. K.; Miller, G. J. *Chem. Mater.* **1990**, *2*, 12–26.
(7) Kranenberg, C.; Johrendt, D.; Mewis, A. *Z. Anorg. Allg. Chem.* **1999**, *625*, 1787–1793.
(8) Kranenberg, C.; Johrendt, D.; Mewis, A. *Solid State Sci.* **2002**, *4*, 261–265.
(9) Wartenberg, F.; Kranenberg, C.; Pocha, R.; Johrendt, D.; Mewis, A.; Hoffmann, R.-D.; Mosel, B. D.; Pöttgen, R. *Z. Naturforsch. B: J. Chem. Sci.* **2002**, *57*, 1270–1276.
(10) Alemany, P.; Llunell, M.; Canadell, E. *J. Comput. Chem.* **2008**, *29*, 2144–2153.
(11) Gascoin, F.; Ottensmann, S.; Stark, D.; Haïle, S. M.; Snyder, G. J. *Adv. Funct. Mater.* **2005**, *15*, 1860–1864.
(12) Wang, X.-J.; Tang, M.-B.; Chen, H.-H.; Yang, X.-X.; Zhao, J.-T.; Burkhardt, U.; Grin, Yu. *Appl. Phys. Lett.* **2009**, *94*, 092106–1–092106–3.
(13) Flage-Larsen, E.; Diplas, S.; Prytz, Ø.; Toberer, E. S.; May, A. F. *Phys. Rev. B* **2010**, *81*, 205204–1–205204–7.
(14) Guo, K.; Cao, Q.-G.; Feng, X.-J.; Tang, M.-B.; Chen, H.-H.; Guo, X.; Chen, L.; Grin, Yu.; Zhao, J.-T. *Eur. J. Inorg. Chem.* **2011**, 4043–4048.
(15) May, A. F.; McGuire, M. A.; Singh, D. J.; Ma, J.; Delaire, O.; Huq, A.; Cai, W.; Wang, H. *Phys. Rev. B* **2012**, *85*, 035202–1–035202–10.
(16) Blanchard, P. E. R.; Stoyko, S. S.; Cavell, R. G.; Mar, A. *J. Solid State Chem.* **2011**, *184*, 97–103.
(17) He, H.; Tyson, C.; Bobev, S. *Inorg. Chem.* **2011**, *50*, 8375–8383.
(18) Stoyko, S. S.; Khatun, M.; Mar, A. *Inorg. Chem.* **2012**, *51*, 9517–9521.
(19) Sheldrick, G. M. *SHELXTL*, v 6.12; Bruker AXS Inc., Madison, WI, 2001.
(20) Gladyshevskii, E. I.; Kripyakevich, P. I.; Bodak, O. I. *Ukr. Fiz. Zh.* **1967**, *12*, 447–452.
(21) Ban, Z.; Sikirica, M. *Acta Crystallogr.* **1965**, *18*, 594–599.
(22) Leciejewicz, J.; Siek, S.; Szytuła, A. *J. Less-Common Met.* **1988**, *144*, L9–L13.
(23) Gaultois, M. W.; Grosvenor, A. P.; Blanchard, P. E. R.; Mar, A. *J. Alloys Compd.* **2010**, *492*, 19–25.
(24) Blanchard, P. E. R.; Cavell, R. G.; Mar, A. *J. Alloys Compd.* **2010**, *505*, 17–22.
(25) Gelato, L. M.; Parthé, E. *J. Appl. Crystallogr.* **1987**, *20*, 139–143.
(26) Tank, R.; Jepsen, O.; Burkhardt, A.; Andersen, O. K. *TB-LMTO-ASA* Program, v 4.7; Max Planck Institut für Festkörperforschung, Stuttgart, Germany, 1998.
(27) Stoyko, S. S.; Mar, A. *J. Solid State Chem.* **2011**, *184*, 2360–2367.
(28) Stoyko, S. S.; Mar, A. *Inorg. Chem.* **2011**, *50*, 11152–11161.
(29) Eisenmann, B.; Klein, J.; Somer, M. *Z. Kristallogr.* **1991**, *197*, 267–268.
(30) Eisenmann, B.; Klein, J.; Somer, M. *Z. Kristallogr.* **1991**, *197*, 265–266.
(31) Eisenmann, B.; Rössler, U. *Z. Kristallogr. – New Cryst. Struct.* **2000**, *215*, 347.
(32) Pauling, L. *The Nature of the Chemical Bond*, 3rd ed.; Cornell University Press: Ithaca, NY, 1960.
(33) Slater, J. C. *J. Chem. Phys.* **1964**, *41*, 3199–3204.
(34) Hoffmann, R.; Zheng, C. *J. Phys. Chem.* **1985**, *89*, 4175–4181.
(35) Hoffmann, R. *Solids and Surfaces: A Chemist's View of Bonding in Extended Structures*; VCH Publishers: New York, 1998.
(36) Huheey, J. E.; Keiter, E. A.; Keiter, R. L. *Inorganic Chemistry: Principles of Structure and Reactivity*, 4th ed.; Harper Collins: New York, 1993.
(37) Johrendt, D.; Felser, C.; Jepsen, O.; Andersen, O. K.; Mewis, A.; Rouxel, J. *J. Solid State Chem.* **1997**, *130*, 254–265.
(38) Gustenau, E.; Herzing, P.; Neckel, A. *J. Solid State Chem.* **1997**, *129*, 147–156.
(39) Kang, D.-B. *Bull. Korean Chem. Soc.* **2003**, *24*, 1215–1218.
(40) An, J.; Sefat, A. S.; Singh, D. J.; Du, M.-H. *Phys. Rev. B* **2009**, *79*, 075120–1–075120–6.
(41) Singh, D. J. *Phys. Rev. B* **2009**, *79*, 153102–1–153102–4.
(42) Chefki, M.; Abd-Elmeguid, M. M.; Micklitz, H.; Huhnt, C.; Schlabitz, W.; Reehuis, M.; Jeitschko, W. *Phys. Rev. Lett.* **1998**, *80*, 802–805.
(43) Kovnir, K.; Thompson, C. M.; Zhou, H. D.; Wiebe, C. R.; Shatruk, M. *Chem. Mater.* **2010**, *22*, 1704–1713.
(44) Brock, S. L.; Greedan, J. E.; Kauzlarich, S. M. *J. Solid State Chem.* **1994**, *109*, 416–418.
(45) Shannon, R. D. *Acta Crystallogr., Sect. A* **1976**, *32*, 751–767.
(46) Imai, M.; Abe, H.; Yamada, K. *Inorg. Chem.* **2004**, *43*, 5186–5188.